

Control of the molecular geometry and nanoscale morphology in perylene diimide based bulk heterojunctions enables an efficient non-fullerene organic solar cell

R. Singh^{a, †}, J. Lee^{a, †}, M. Kim^a, P. E. Keivanidis^{b,*}, K. Cho^{a,*}

^a Department of Chemical Engineering, Pohang University of Science and Technology, Pohang, 790–784, Korea

^b Department of Mechanical Engineering and Materials Science and Engineering Cyprus University of Technology Dorothea Bldg, 5th floor 45 Kitiou Kyprianou str., Limassol 3041, Cyprus

[†] Dr. R. Singh and J. Lee contributed equally to this work.

* Prof. Kilwon Cho, kwcho@postech.ac.kr

* Asst. Prof. Panagiotis E. Keivanidis, p.keivanidis@cut.ac.cy

I. Experimental section.

1. Materials and Methods:

Materials All reagents and chemicals were purchased from commercial sources and used without further purification. All anhydrous organic solvents for the synthesis, characterization, and device fabrication steps, including tetrahydrofuran, dimethyl sulfoxide, chloroform, and chlorobenzene were purchased from Sigma-Aldrich, TCI, and Alfa Aesar. 1-Hexylheptylamine,^[1] *N,N'*-bis(1-hexylheptyl)perylene-3,4,9,10-tetracarboxylbisimide (PDI1),^[1] 1Br-PDI1,^[2] PDI2,^[3] and PDI4^[4] were synthesized using modified literature procedure.

Characterizations of compounds ¹H spectra of intermediate monomers were recorded on a Bruker AVANCE 400 MHz NMR spectrometer. PDI1, PDI2, and PDI4 were characterized by ¹H NMR (500 MHz) on Bruker DRX 500 spectrometer. Mass spectra were obtained from Bruker Reflex III Matrix-Assisted LASER Desorption Ionization - Time of Flight Mass Spectrometer (MALDI-TOF) using α -Cyano-4-hydroxycinnamic acid (α -CCA) as a matrix^[5] recorded in a (+)-reflector mode. Elemental analysis was performed by Vario MICRO.

Electrochemical characterizations The electrochemical cyclic voltammetry (CV) was conducted on a PowerLab/AD instrument model system with glassy carbon disk, Pt wire, and Ag/Ag⁺ electrode as the working electrode, counter electrode, and reference electrode, respectively in a 0.1 M tetrabutylammonium hexafluorophosphate (*n*-Bu₄NPF₆)-anhydrous acetonitrile solution at a potential scan rate of 50 mV s⁻¹. Thin films of samples were deposited onto the glassy carbon working electrode from a 2.0 mg mL⁻¹ chloroform solution. The electrochemical onsets were determined at the position where the current starts to differ from the baseline. The potential of

Ag/AgCl reference electrode was internally calibrated by using the ferrocene/ferrocenium redox couple (Fc/Fc⁺). The electrochemical energy levels were estimated by using the empirical formula:

$$E_{\text{HOMO}} = -(4.80 + E_{\text{onset, ox}}) \text{ and } E_{\text{LUMO}} = -(4.80 + E_{\text{onset, red}}).^{[6]}$$

Computational studies Density functional theory (DFT) calculations were performed to facilitate an in-depth understanding of the electronic structure of the polymer by Gaussian 09 software package.^[7] Hybrid three-parameter B3LYP functional combined with 6-31G(d) basis set was used to obtain the optimized structures at the singlet ground state.^[8] For simplicity, the alkyl chains were trimmed with methyl chains. The highest occupied molecular orbital (HOMO) as well as lowest unoccupied molecular orbital (LUMO) energy levels were analyzed using minimized singlet geometries to approximate the ground state.

Fabrication and characterization of organic solar cell (OSC) devices The inverted structure of the OSC devices was prepared with stack glass / indium tin oxide (ITO) (110nm) / zinc oxide (ZnO) (40nm) /polymer:PDI_s (95 - 100nm) / V₂O₅ (2nm) / Ag (100nm). ITO-coated glass substrates were cleaned by sequential sonications with detergent, distilled water, acetone, and isopropyl alcohol for 15 min at each step. After UV/ozone treatment for 30 min, a ZnO electron transport layer^[9] was prepared by spin-coating at 4000 rpm and then baked at 120 °C for 30 min on the hot plate in ambient condition. Active layer solutions were prepared in CB (polymer concentration: 7.6 mg mL⁻¹) and kept on a hotplate at 70 °C for 12 hours. Active layers were spin-coated from the warm polymer solution on the prepared glass/ITO/ZnO substrate in a N₂ glovebox, and then the films were annealed at 90 °C for 5 minutes. To deposit the electrodes, the samples were transferred into a vacuum chamber (pressure < 2×10⁻⁶ Torr), and then V₂O₅ (2 nm)/Ag (100 nm) were thermally deposited sequentially on top of the active layer with the help of shadow mask.

The device area was 0.0555 cm². The electrical characteristics were measured with a source/measure unit (Keithley 4200) under 100 mW cm⁻² AM1.5 solar illumination in a N₂-filled glove box. Light was generated with an Oriel 1-kW solar simulator referenced using a Reference Cell PVM 132 calibrated at the US National Renewable Energy Laboratory. A photomodulation spectroscopic set-up (model Merlin, Oriel) was used to measure the incident photon-to-current conversion efficiency as a function of light wavelength.

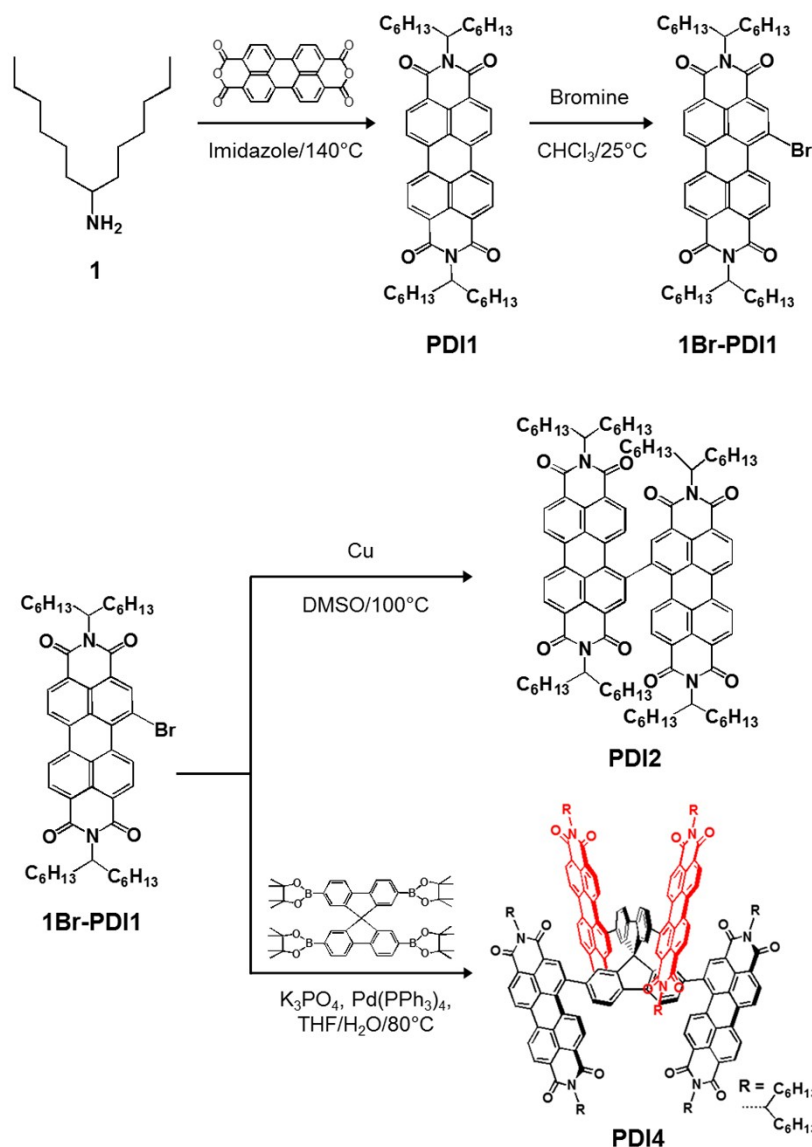
Morphology characterization: Atomic force microscopy (AFM) and transmission electron microscopy (TEM) images were obtained using a MultiMode 8 Scanning Probe Microscope VEECO Instruments Inc. and JEOL JEM-2200FS (with Image Cs-corrector), respectively.

Grazing incidence wide angle X-ray scattering (GIWAXS) analysis GIWAXS measurements were performed using Beam-line 3C at the Pohang Accelerator Laboratory (PAL). The photon energy is 10.6408 keV ($\lambda = 1.1651 \text{ \AA}$). The GIWAXS images shown are normalized with respect to the exposure time.

SCLC measurement The hole and electron mobility data was extracted from the dark $J-V$ characteristics of hole-only devices, ITO/PEDOT:PSS/polymer:PDIs/Au, and electron-only devices ITO/ZnO/polymer:PDIs/Ca/Al devices. The electrical characteristics were measured with a source/measure unit (Keithley 4200) in a N₂-filled glove box. The dark $J-V$ curves were fitted by using the Mott-Gurney equation (eq. 1)^[10],

$$J(V) = \frac{9}{8} \varepsilon_0 \varepsilon_r \mu_0 \exp(0.89 \gamma \sqrt{V/L}) \frac{V^2}{L^3} \quad (1)$$

where J is the dark current density, ϵ_0 is the vacuum permittivity, ϵ_r is the relative dielectric constant, μ_0 is the zero-field mobility, γ is the disorder parameter, V is the effective voltage and L is the film thickness. For the case of hole-only devices the built in voltage (V_{bi}) value of 0V and for electron-only devices $V_{bi} = 1.5$ V was used.



Scheme S1. Synthetic procedure of PDI1, PDI2, and PDI4. ffffff

PDI1: A mixture of perylene-3,4,9,10-tetracarboxylic dianhydride (1.95 g, 5.0 mmol), 1-hexylheptylamine (2.49 g, 12.5 mmol), and imidazole (10.0 g) were stirred overnight at 140°C. The reaction mixture was cooled to room temperature, taken up in 150 mL ethanol, treated with 200 mL 2M HCl, and stirred for 6h. The dark red precipitate was filtered and washed with distilled water. The compound was purified by silica gel column chromatography (*n*-hexane:chloroform = 1:3) to afford the product as dark yellow solid (3.23 g, 86%).

^1H NMR (400 MHz, CDCl_3 , ppm): δ 8.64 (m, 8H), 5.19 (m, 2H), 2.25 (m, 4H), 1.87 (m, 4H), 1.30–1.18 (m, 32H), 0.83 (t, 12H).

Elem. Anal. Calcd for $\text{C}_{50}\text{H}_{62}\text{N}_2\text{O}_4$: C, 79.54; H, 8.28; N, 3.71. Found: C, 79.48; H, 8.30; N, 3.76.

1Br-PDI1: To a 3-neck round flask charged with a solution of compound **2** (3.0 g, 4.0 mmol) in CHCl_3 (100 mL) was added bromine (10 mL) and stirred at room temperature for 60 h. After the excess of bromine was removed by a gentle stream of air, the organic mixture was washed with aqueous Na_2SO_3 and aqueous Na_2CO_3 sequentially. Then, the organic layer was dried over Na_2SO_4 and concentrated in vacuo. The residue was purified by silica gel column chromatography (*n*-hexane:chloroform = 1:1 to 1:3, v/v) to afford the product as dark yellow solid (1.3 g, 42%).

^1H NMR (400 MHz, CDCl_3 , ppm): δ 9.81 (d, 1H), 8.93 (s, 1H), 8.75–8.62 (m, 5H), 5.18 (m, 2H), 2.24 (m, 4H), 1.85 (m, 4H), 1.33–1.18 (m, 32H), 0.83 (t, 12H).

PDI2: To a 3-neck round flask charged with a solution of 1Br-PDI1 (0.6 g, 0.72 mmol) in dry DMSO (50 mL) was added copper powder (Alfa Aesar, <100 nm particle size, 99.8%) (520 mg, 7.2 mmol) and stirred at 100 °C for 5 h. The cooled mixture was poured into water and extracted with CH_2Cl_2 several times. Then, the organic layer was dried over Na_2SO_4 and concentrated in vacuo. The residue was purified by silica gel column chromatography (chloroform) to afford the product as red-violet solid (0.82 g, 75.6%).

^1H NMR (400 MHz, CDCl_3 , ppm): δ 8.82–8.77 (m, 8H), 8.50 (d, 2H), 8.16 (m, 4H), 5.14–5.00 (m, 4H), 2.20–2.04 (m, 8H), 1.90–1.72 (m, 8H), 1.24 (m, 64H), 0.78 (s, 24H).

Elem. Anal. Calcd for $\text{C}_{100}\text{H}_{122}\text{N}_4\text{O}_8$: C, 79.64; H, 8.15; N, 3.72. Found: C, 79.57; H, 8.23; N, 3.75.

PDI4: A mixture of 2,2',7,7'-tetrakis(4,4,5,5-tetramethyl-1,3,2-dioxaborolan-2-yl)-9,9'-spirobi[fluorene] (150 mg, 0.18 mmol), 1Br-PDI1 (640 mg, 0.76 mmol), $\text{Pd}(\text{PPh}_3)_4$ (60 mg, 0.053 mmol), K_3PO_4 aqueous solution (1 M, 1 mL), THF (10 mL) and water (3 mL) was heated to 80 °C for 50 h under N_2 . After cooling to room temperature, the reaction mixture was poured into 100 mL NaCl aqueous solution and extracted with dichloromethane three times (50 mL \times 3). The

organic layer was dried over Na_2SO_4 and concentrated in vacuo. The residue was purified by silica gel column chromatography two times (1st: chloroform and 2nd: *n*-hexane:ethyl acetate = 9:1) to afford the product as deep red solid (383 mg, 63%).

^1H NMR (400 MHz, *o*-dichlorobenzene- d_4 , ppm): δ 8.60–8.45 (m, 12H), 8.33–8.19 (m, 16H), 7.73–7.45 (m, 12H), 5.35–5.08 (m, 8H), 2.33–1.81 (m, 32H), 1.50–0.98 (m, 128H), 0.90–0.58 (m, 48H).

MS (MALDI-TOF): m/z (M^+) = Calcd for $\text{C}_{225}\text{H}_{256}\text{N}_8\text{O}_{16}$: 3325.9; found 3326.9.

Elem. Anal. Calcd for $\text{C}_{225}\text{H}_{256}\text{N}_8\text{O}_{16}$: C, 81.19; H, 7.75; N, 3.37. Found: C, 81.21; H, 7.63; N, 3.13.

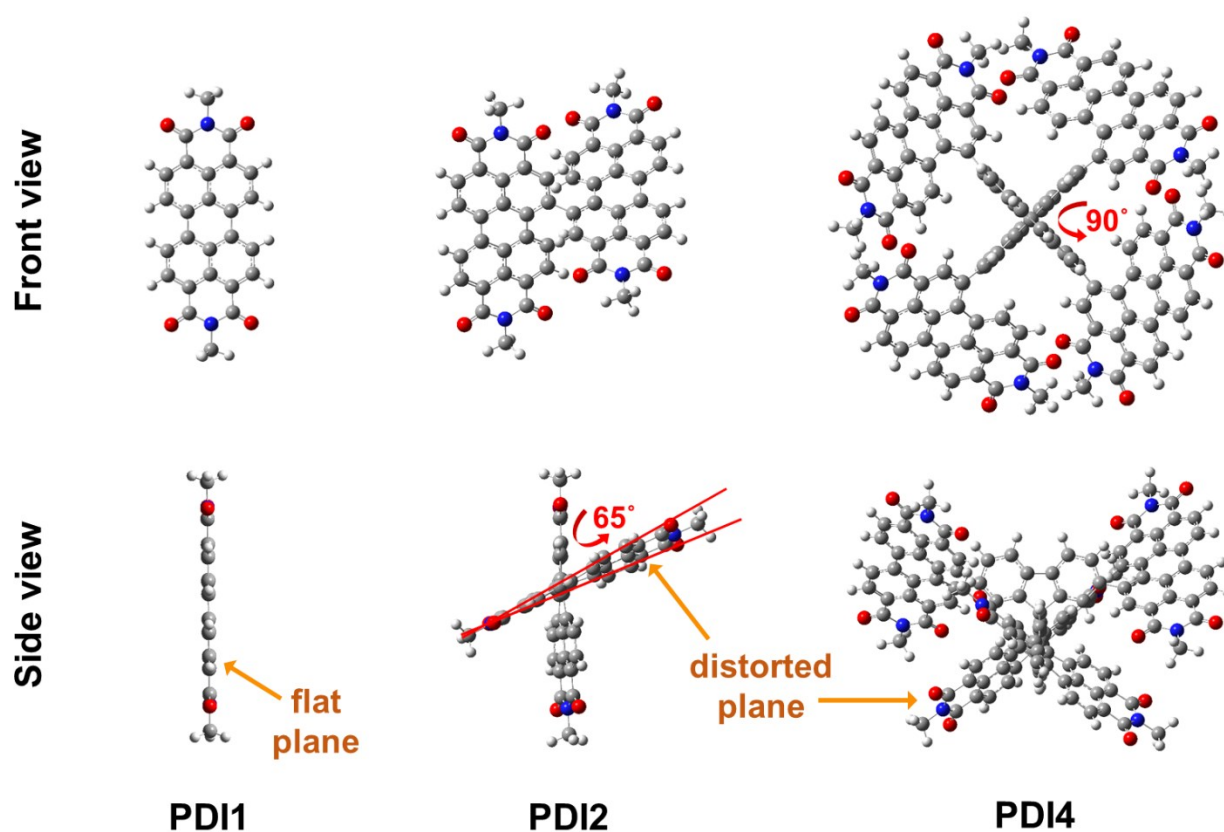


Figure S1. Energy-minimized structural conformation of PDI1, PDI2, and PDI4 using DFT calculation (B3LYP functional/6-31G* basis set).

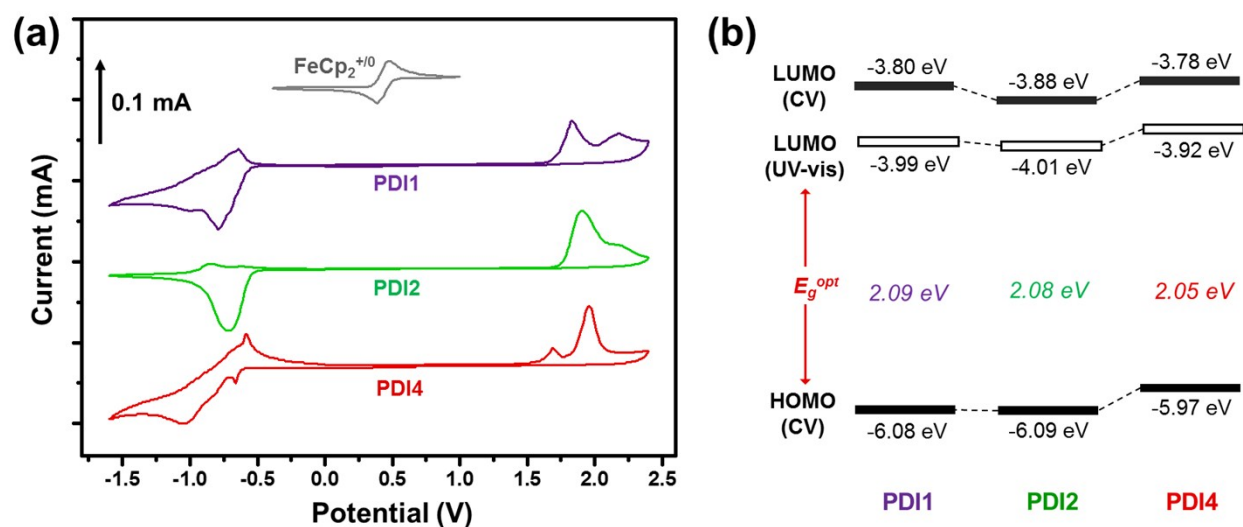


Figure S2. (a) Cyclic voltammograms and (b) energy diagrams of PDI1, PDI2, and PDI4.

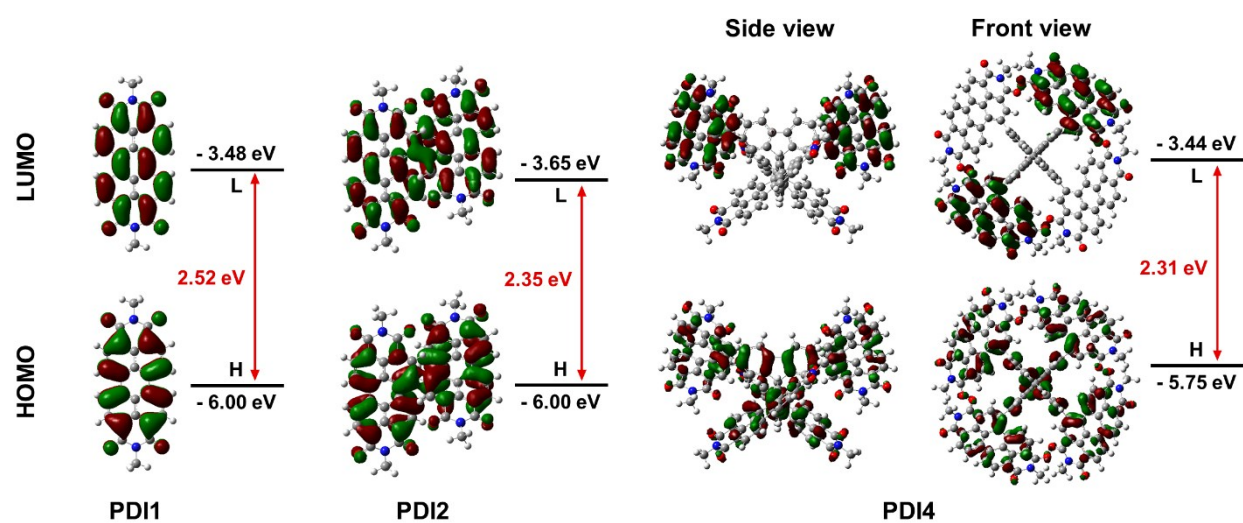


Figure S3. Frontier molecular orbitals and energy level diagrams of PDI1, PDI2, and PDI4 measured by DFT calculation (B3LYP functional/6-31G* basis set). Methyl-trimmed alkyl chains were used for simplicity of computation.

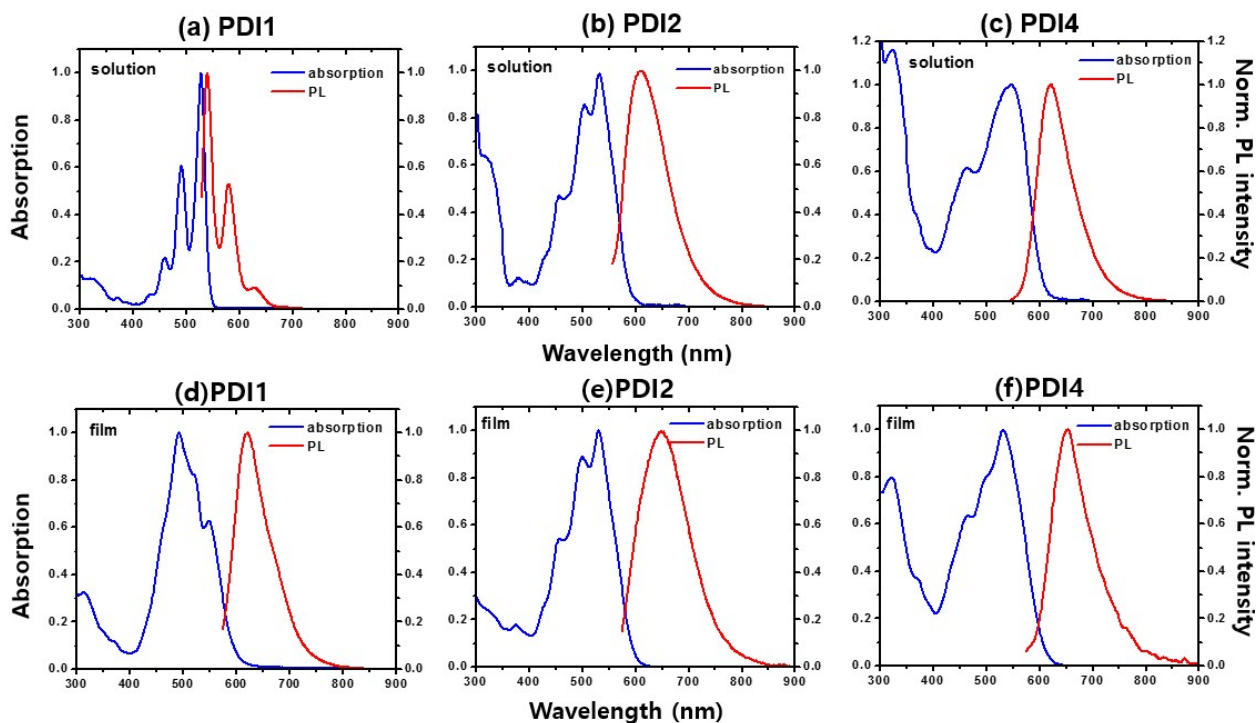


Figure S4. UV-vis absorption and photoluminescence spectra (PL) for dilute solution of a) PDI1 (331 nM molar concentration), b) PDI2 (166 nM molar concentration) and c) PDI4 (75 nM molar concentration) in chlorobenzene (CB), and for spin-coated thin films of d) PDI1, e) PDI2 and f) PDI4 spun from CB.

Table S1. Properties of PDI1, PDI2, and PDI4.

Materials	$\lambda_{\max}^{\text{film}}$	$E_g^{\text{film, opt}}$	$E_{\text{HOMO}}^{\text{CV}}$	$E_{\text{LUMO}}^{\text{CV}}$	$E_g^{\text{film, CV}}$	$E_{\text{LUMO}}^{\text{opt}}$
		[eV] ^a	[eV] ^b	[eV] ^b		[eV] ^c
PDI1	492, 523, 548	2.09	-6.08	-3.80	-2.28	3.99
PDI2	456, 499, 531	2.08	-6.09	-3.88	-2.21	-4.01
PDI4	462, 498, 532	2.05	-5.97	-3.78	-2.19	-3.92

^a Optical band gaps, calculated from the absorption edges. ^b Calculated from the onsets of oxidation and reduction potential measured by CV. ^c The LUMO energy levels were estimated from the HOMO energy levels (CV) and the optical band gaps (UV-vis) in the solid state by using the following equation: $E_{\text{LUMO}} = E_g^{\text{opt}} + E_{\text{HOMO}}$.^[6]

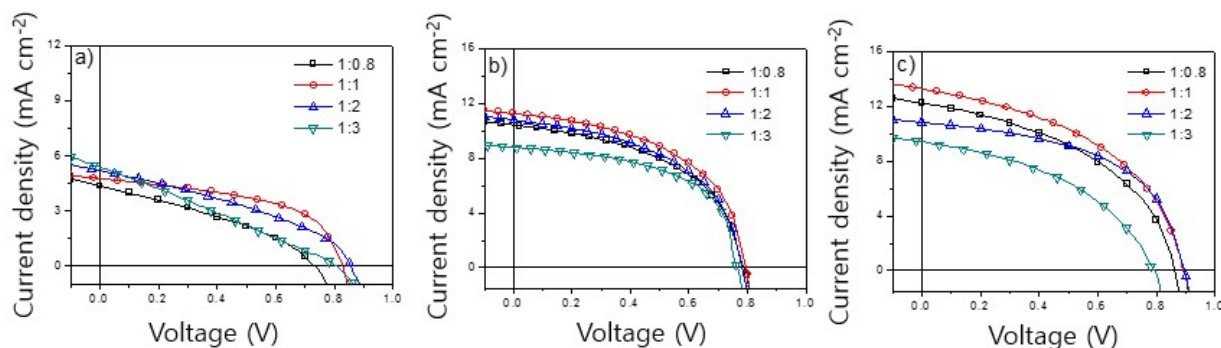


Figure S5. J–V characteristics of (a) PTB7-Th:PDI1, (b) PTB7-Th:PDI2 and (c) PTB7-Th:PDI4 with different D:A compositions.

Table S2. Photovoltaic properties of the solar cells based on PTB7-Th:PDI1, PTB7-Th:PDI2 and PTB7-Th:PDI4 with different D:A compositions

D:A	Voc (Volts)	Jsc (mA cm ⁻²)	FF (%)	PCE _{avg} (%)	PCE _{max} (%)
PTB7-Th:PDI1 (1:0.8)	0.74 ± 0.016	4.35 ± 0.08	34.7 ± 1.42	1.11 ± 0.20	1.31
PTB7-Th:PDI1 (1:1)	0.82 ± 0.007	4.76 ± 0.12	52.1 ± 1.15	2.04 ± 0.05	2.09
PTB7-Th:PDI1 (1:2)	0.82 ± 0.009	5.18 ± 0.08	39.7 ± 0.74	1.68 ± 0.11	1.79
PTB7-Th:PDI1 (1:3)	0.81 ± 0.006	5.37 ± 0.09	25.6 ± 0.85	1.08 ± 0.08	1.16
PTB7-Th:PDI2 (1:0.8)	0.78 ± 0.004	10.43 ± 0.16	50.1 ± 0.09	4.10 ± 0.08	4.18
PTB7-Th:PDI2 (1:1)	0.78 ± 0.004	11.38 ± 0.10	49.8 ± 0.17	4.39 ± 0.12	4.51
PTB7-Th:PDI2 (1:2)	0.78 ± 0.008	10.78 ± 0.13	49.3 ± 0.14	4.16 ± 0.06	4.22
PTB7-Th:PDI2 (1:3)	0.77 ± 0.004	8.01 ± 0.12	50.6 ± 0.11	3.15 ± 0.14	3.29
PTB7-Th:PDI4 (1:0.8)	0.86 ± 0.007	12.14 ± 0.08	46.1 ± 0.16	4.78 ± 0.11	4.89
PTB7-Th:PDI4 (1:1)	0.90 ± 0.01	13.25 ± 0.14	47.6 ± 0.62	5.58 ± 0.08	5.66
PTB7-Th:PDI4 (1:2)	0.90 ± 0.003	10.81 ± 0.6	52.6 ± 0.33	5.12 ± 0.13	5.25
PTB7-Th:PDI4 (1:3)	0.80 ± 0.002	9.42 ± 0.12	42.3 ± 0.17	3.18 ± 0.26	3.44

Table S3. Photovoltaic properties of the fabricated OSC devices with PTB7-Th:PDIs photoactive layers in different DIO additive volume % (0.5%, 0.7%, 1% and 2%).

Sample	Voc (Volts)	Jsc (mA cm ⁻²)	FF (%)	PCE _{avg} (%)	PCE _{max} (%)
PTB7-Th:PDI1 w/ 0.5% DIO	0.80 ± 0.01	4.88 ± 0.27	60.2 ± 1.42	2.35 ± 0.13	2.48
PTB7-Th:PDI1 w/ 0.7% DIO	0.81 ± 0.004	5.06 ± 0.12	50.2 ± 1.12	2.01 ± 0.08	2.09
PTB7-Th:PDI1 w/ 1% DIO	0.81 ± 0.002	4.56 ± 0.08	47.6 ± 0.83	1.75 ± 0.11	1.86
PTB7-Th:PDI1 w/ 2% DIO	0.81 ± 0.005	3.81 ± 0.13	41.1 ± 1.15	1.26 ± 0.05	1.31
PTB7-Th:PDI2 w/ 0.5% DIO	0.77 ± 0.001	12.31 ± 0.13	50.3 ± 0.16	4.78 ± 0.11	4.89
PTB7-Th:PDI2 w/ 0.7% DIO	0.76 ± 0.006	13.01 ± 0.16	53.3 ± 0.62	5.27 ± 0.02	5.32
PTB7-Th:PDI2 w/ 1% DIO	0.77 ± 0.001	12.78 ± 0.10	51.1 ± 0.16	5.03 ± 0.16	5.19
PTB7-Th:PDI1w/ 2% DIO	0.77 ± 0.004	12.41 ± 0.07	46.8 ± 0.16	4.47 ± 0.14	4.61
PTB7-Th:PDI4 w/ 0.5% DIO	0.90 ± 0.001	13.06 ± 0.10	52.3 ± 0.33	6.13 ± 0.9	6.22
PTB7-Th:PDI4w/ 0.7% DIO	0.90 ± 0.005	13.36 ± 0.05	53.6 ± 0.33	6.32 ± 0.13	6.44
PTB7-Th:PDI4 w/ 1% DIO	0.90 ± 0.003	12.97 ± 0.07	51.6 ± 0.33	6.04 ± 0.12	6.16
PTB7-Th:PDI4 w/ 2% DIO	0.90 ± 0.004	12.56 ± 0.12	49.3 ± 0.33	5.62 ± 0.16	5.78

Table S4. Short circuit current density (J_{SC}) and calculated J_{SC} from the EQE spectrum of OSC devices for the PTB7-Th:PDI1 w/o DIO, PTB7-Th:PDI2 w/o DIO, PTB7-Th:PDI4 w/o DIO, PTB7-Th:PDI1 w/ DIO, PTB7-Th:PDI2 w/ DIO and PTB7-Th:PDI4 w/ DIO.

D:A	J_{SC} (mA cm ⁻²)	$J_{SC(EQE)}$ (mA cm ⁻²)
PTB7-Th:PDI1 w/o DIO	4.76 ± 0.12	4.56
PTB7-Th:PDI2 w/o DIO	11.38 ± 0.10	11.27
PTB7-Th:PDI4 w/o DIO	13.25 ± 0.14	13.01
PTB7-Th:PDI1 w/ DIO	4.88 ± 0.27	4.87
PTB7-Th:PDI2 w/ DIO	13.01 ± 0.16	12.87
PTB7-Th:PDI4 w/ DIO	13.36 ± 0.05	13.24

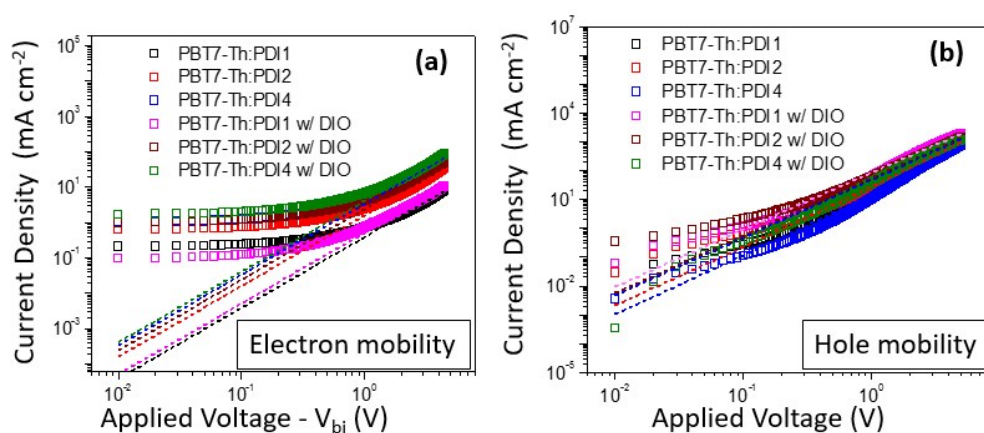


Figure S6. Dark current density versus effective voltage characteristics of a) electron-only devices and b) hole-only devices, with photoactive layers PTB7-Th:PDI1, PTB7-Th:PDI2 and PTB7-Th:PDI4 w/o DIO and w/ DIO. The dotted lines are fits based on Mott-Gurney equation. In the case of electron-only devices the $V_{bi} = 1.5$ V is used.

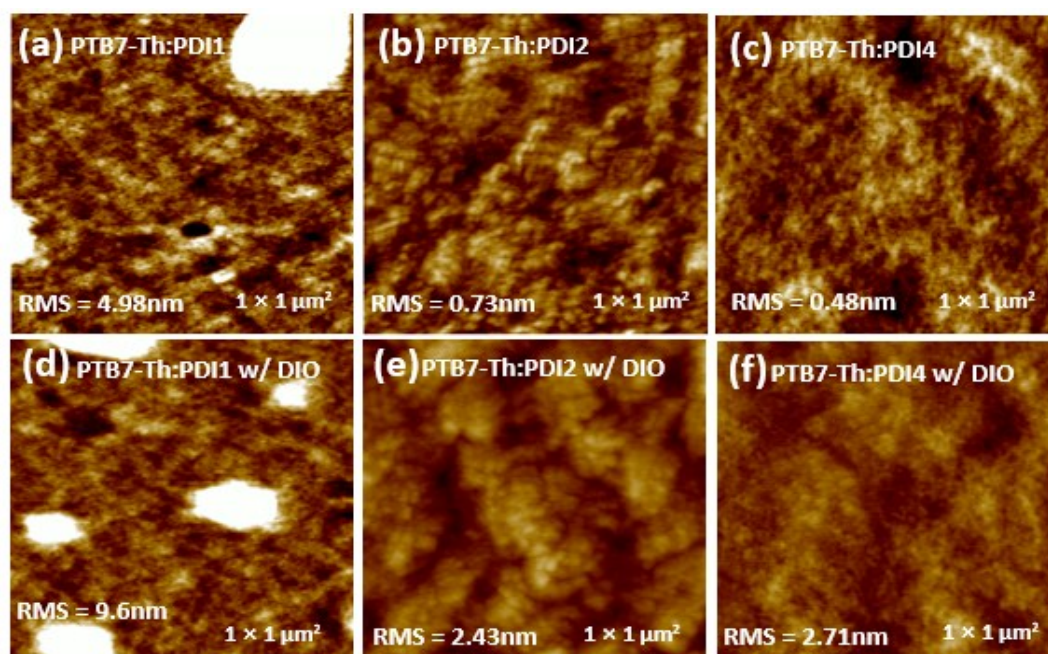


Figure S7. AFM height images of blend films based on PTB7-Th:PDI1, PTB7-Th:PDI2 and PTB7-Th:PDI4 (a-c) and blend w/ DIO (d-f).

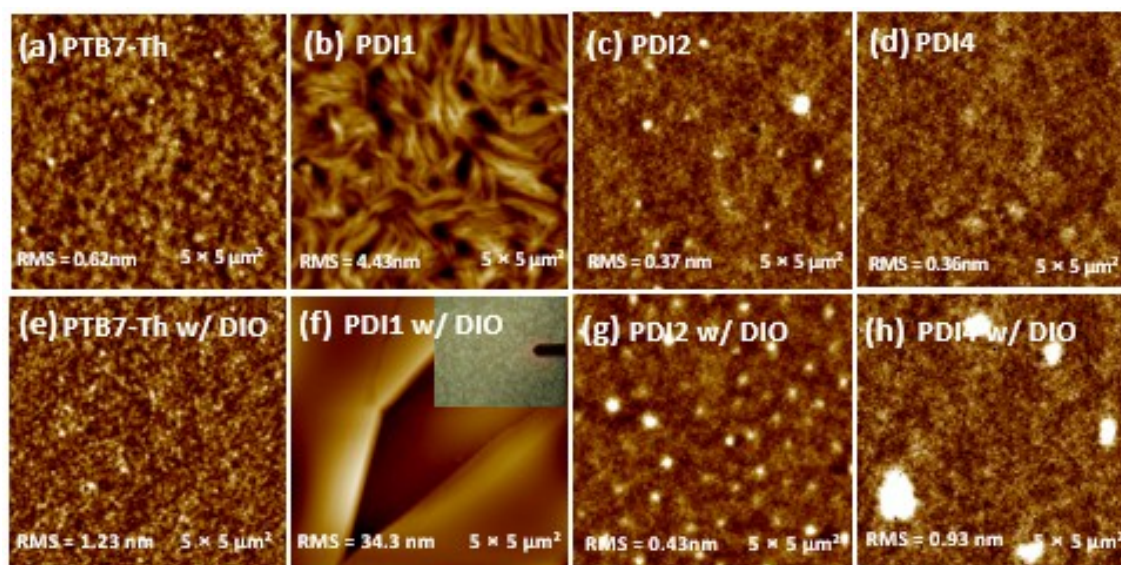


Figure S8. AFM height images for the neat films of PTB7-Th, PDI1, PDI2 and PDI4 (a-d) and PDI4, PTB7-Th, PDI1, PDI2 and PDI4 w/ DIO (e-h). In figure (f), inset microscopic image was captured during the AFM measurement.

Table S5. The root mean square (rms) and average roughness values of the surface of the neat and blend films studied in this work.

Sample	R_{RMS} (nm)	R_{avg} (nm)
PTB7-Th	0.62	0.49
PDI1	4.58	3.11
PDI2	0.37	0.31
PDI4	0.36	0.26
PTB7-Th w/ DIO	1.23	0.95
PDI1 w/ DIO	34.3	27.5
PDI2 w/ DIO	0.43	0.27
PDI4 w/ DIO	0.93	0.55
PTB7-Th:PDI1	4.98	3.32
PTB7-Th:PDI2	0.73	0.52
PTB7-Th:PDI4	0.48	0.39
PTB7-Th:PDI1 w/ DIO	9.6	13.62
PTB7-Th:PDI2 w/ DIO	2.43	1.81
PTB7-Th:PDI4 w/ DIO	2.71	2.19

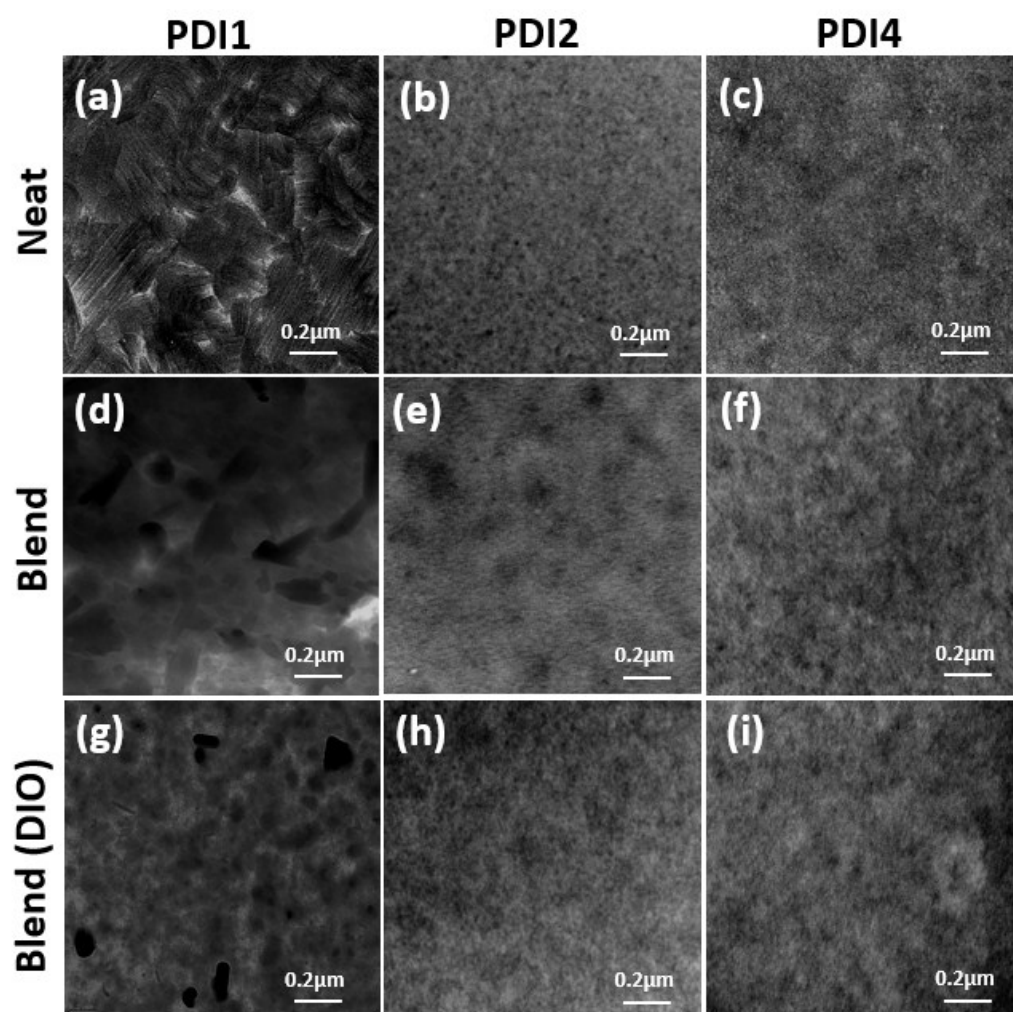


Figure S9. TEM images of films based on neat PDI1, PDI2 and PDI4 (a-c), and PTB7-Th:PDI1, PTB7-Th:PDI2 and PTB7-Th:PDI4 blend films without DIO (d-e) and with DIO (g-i).

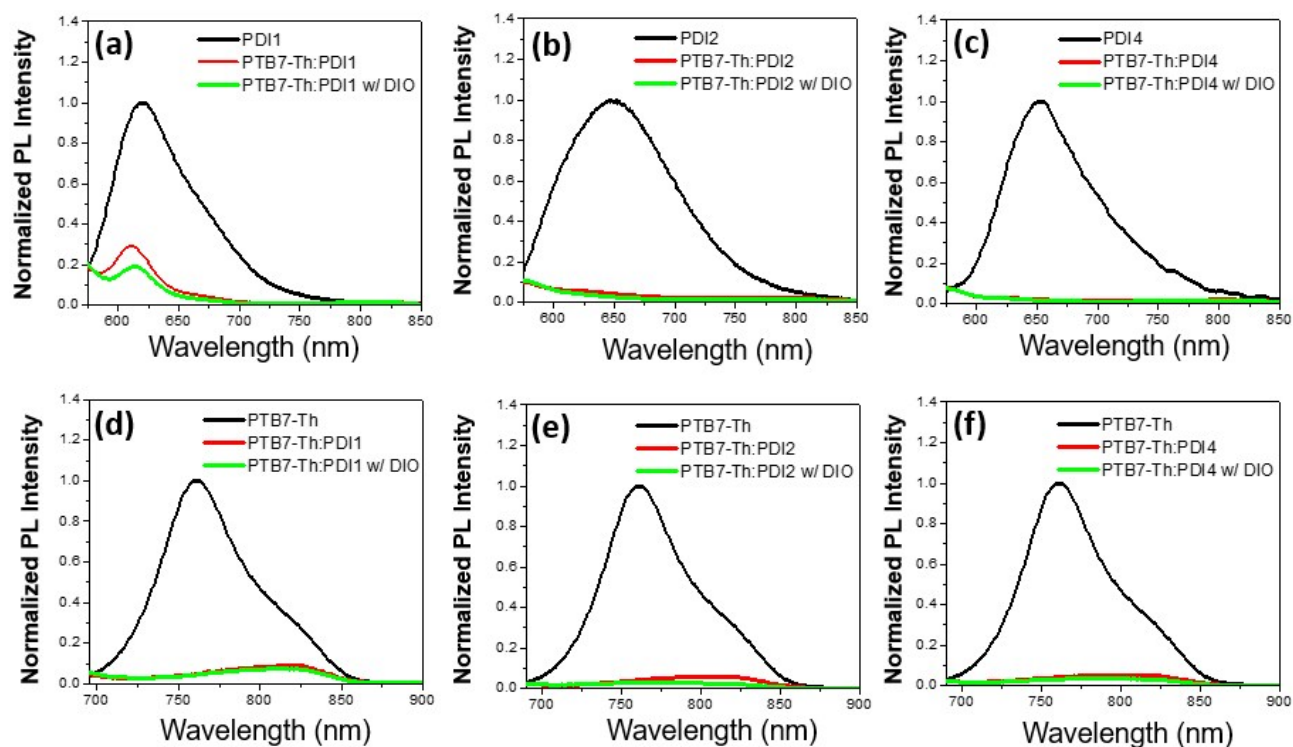


Figure S10. Normalized PL spectra for blend films of (a) PTB7-Th:PDI1, (b) PTB7-Th:PDI2 and (c) PTB7-Th:PDI4 w/o DIO and w/ DIO w.r.t. neat PDI1, PDI2 and PDI4 film where the films were excited at 532 nm. Normalized PL spectra for blend films of (d) PTB7-Th:PDI1 (e) PTB7-Th:PDI2 and (f) PTB7-Th:PDI4 w/o DIO and w/ DIO w.r.t. a neat PTB7-Th film where the films were excited at 631 nm.

Table S6. PL quenching efficiency of the studied blend films w/ and w/o DIO.

D:A	PL Quenching efficiency (%)	
	Quenching induced by electron transfer (excitons from donors)	Quenching induced by hole transfer (excimers from acceptors)
PTB7-Th:PDI1	83.2	79.3
PTB7-Th:PDI2	90.01	92.1
PTB7-Th:PDI4	90.07	94.04
PTB7-Th:PDI1 w/ DIO	83.3	84.9
PTB7-Th:PDI2 w/ DIO	93.5	93.9
PTB7-Th:PDI4 w/ DIO	92.8	94.5

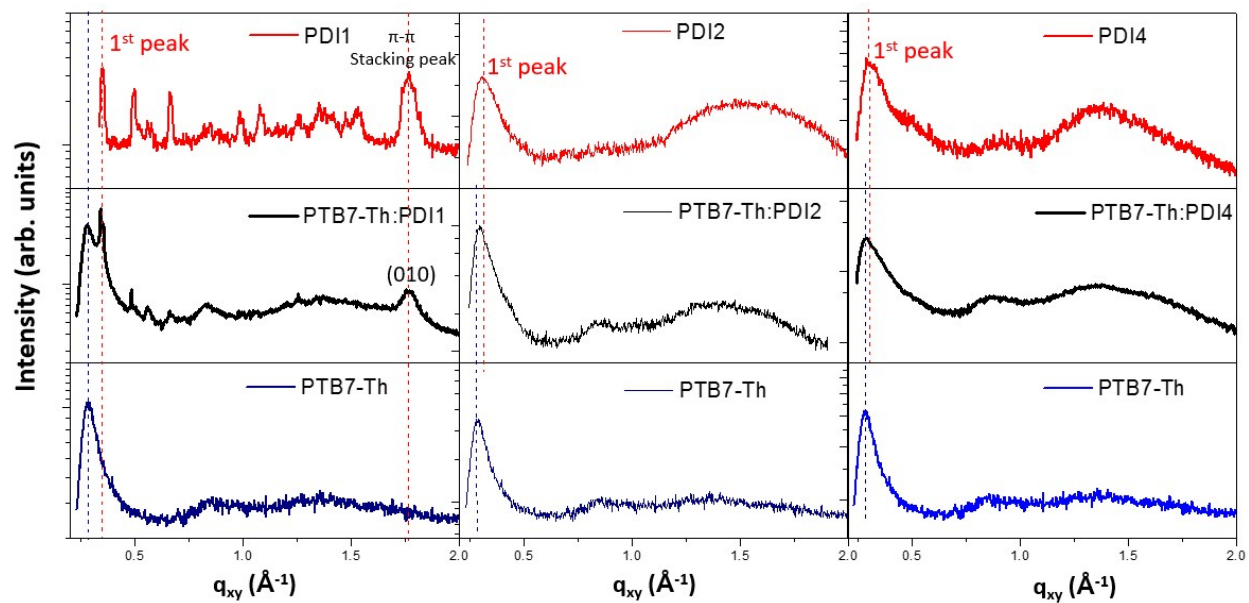


Figure S11. Comparison of polymer (PTB7-Th) and different PDIs (PDI1, PDI2, and PDI4) inplane GIWAXS scan together with respective blend films. Blue and red dashed lines indicate the polymer (100) and PDIs primary (1st) reflections, respectively.

Table S7. GIWAXS results for the neat films of PDI1, PDI2, PDI4, and PTB7-Th.

	Scan	Peak index	peak position (\AA^{-1})	Spacing (\AA)	Coherence Length(\AA)
PTB7-Th	in-plane	(100)	0.29	21.7	95.0
	in-plane	(300)	0.86	7.3	53.3
	out-of-plane	(100) [']	0.29	21.3	48.3
	out-of-plane	(010)	1.52	4.13	19.2
PDI1	in-plane	1 st Peak	0.35	17.84	321.1
	in-plane	π - π stacking peak	1.77	3.55	84.73
	Out-of-plane	1 st Peak	0.35	17.84	341.3
PDI2	in-plane	1 st Peak	0.32	19.6	68.9
	Out-of-plane	1 st peak	0.30	20.9	82.7
PDI4	in-plane	1 st Peak	0.30	20.93	81.7
	Out-of-plane	1 st peak	0.30	20.93	92.25

Table S8. GIWAXS results for the PTB7-Th:PDI1, PTB7-Th:PDI2, PTB7-Th:PDI4 blend films.

	Scan	Peak index	Peak position (\AA^{-1})	Spacing (\AA)	Coherence length (\AA)
PTB7-Th:PDI1					
PTB7-Th	in-plane	(100)	0.28	22.6	114.64
	Out-of-plane	(100)	0.28	22.6	105.1
PDI1	in-plane	1 st Peak	0.340	18.5	305.67
	Out-of-plane	1 st peak	0.35	17.9	122.8
	in-plane	π - π stacking peak	1.76	3.57	73.69
PTB7-Th:PDI2					
PTB7-Th	in-plane	(100)	0.29	21.6	127.04
	Out-of-plane	(100)	0.30	20.9	157.63
PDI2	in-plane	1 st Peak	0.32	19.6	84.3
	Out-of-plane	1 st peak	0.32	19.6	108.9
PTB7-Th:PDI4					
PTB7-Th	in-plane	(100)	0.286	21.9	148.1
	Out-of-plane	(100)	0.282	22.2	110.7
PDI4	in-plane	1 st Peak	0.31	20.3	93.1
	Out-of-plane	1 st peak	0.32	19.6	72.5

Table S9. GIWAXS results for the PTB7-Th:PDI1, PTB7-Th:PDI2, PTB7-Th:PDI4 blend films w/ DIO.

		peak index	peak position (\AA^{-1})	Spacing (\AA)	Coherence length (\AA)
PTB7-Th:PDI1 w/ DIO					
PTB7-Th	in-plane	(100)	0.30	20.9	80.4
	Out-of-plane	(100)	0.26	24.1	135.8
	in-plane	1 st Peak	0.346	18.15	455.8
PDI1	in-plane	π - π stacking peak	1.76	3.56	84.73
	Out-of-plane	1 st peak	0.34	18.5	323.3
PTB7-Th:PDI2 w/ DIO					
PTB7-Th	in-plane	(100)	0.28	22.6	171.9
	Out-of-plane	(100)	0.28	22.6	161.8
PDI2	in-plane	1 st Peak	0.31	20.2	100.9
	Out-of-plane	1 st peak	0.30	20.9	104.6
PTB7-Th:PDI4 w/ DIO					
PTB7-Th	in-plane	(100)	0.28	22.4	152.1
	Out-of-plane	(100)	0.28	22.4	114.7
PDI4	in-plane	1 st Peak	0.31	20.2	106.6
	Out-of-plane	1 st peak	0.32	19.6	67.6

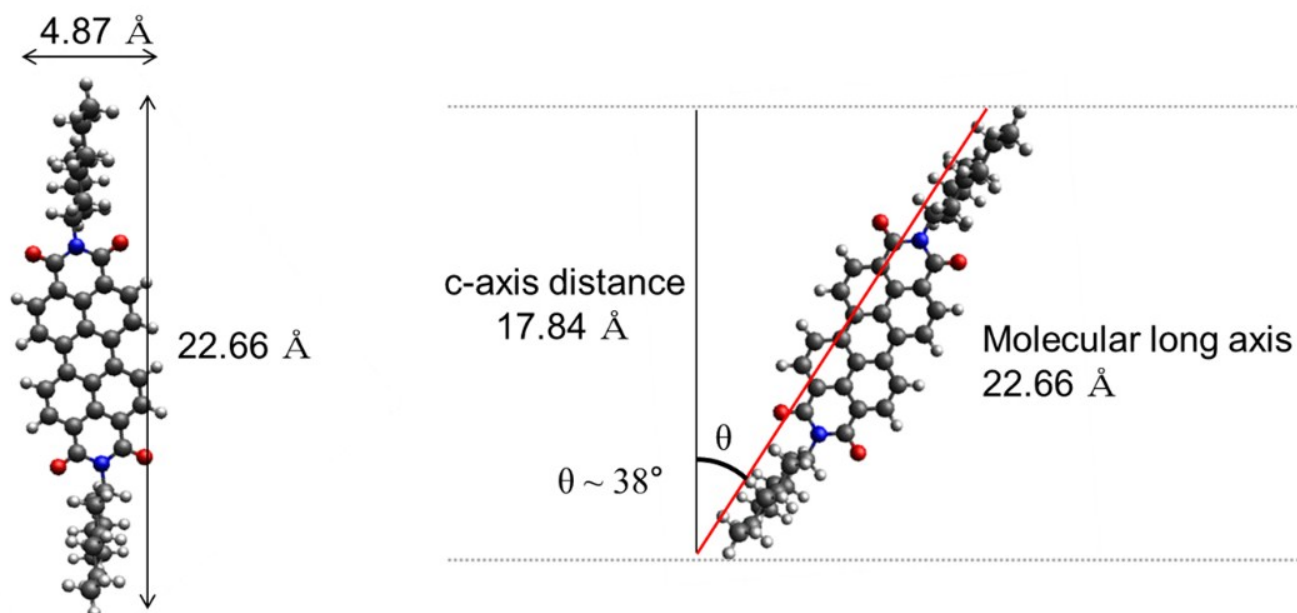


Figure S12. Schematic drawing for a possible structural model of pure PDI1 the molecule on the substrate plane (measured by using Avogadro program).

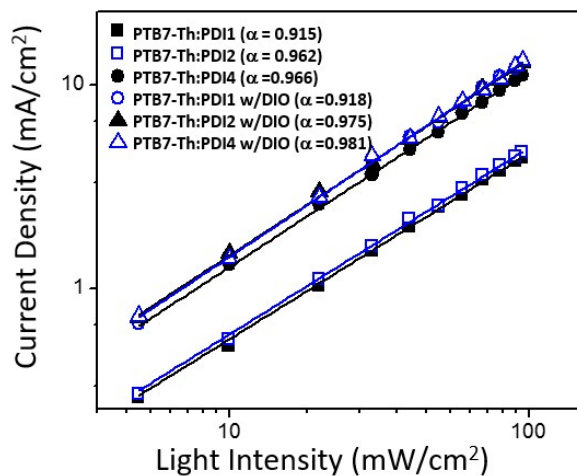


Figure S13. Light intensity (I) dependence current density (J_{SC}) for PTB7-Th:PDI1 without DIO (filled squares, black), PTB7-Th:PDI2 without DIO (filled circles, black), PTB7-Th:PDI4 without DIO (filled up-triangles, black), PTB7-Th:PDI1 with DIO (open squares, blue), PTB7-Th:PDI2 with DIO (open circles, blue) and PTB7-Th:PDI4 with DIO (open up-triangles blue) based OSCs. Solid lines show the fitting for the experimental data with equation, $J_{SC} \propto I^\alpha$.

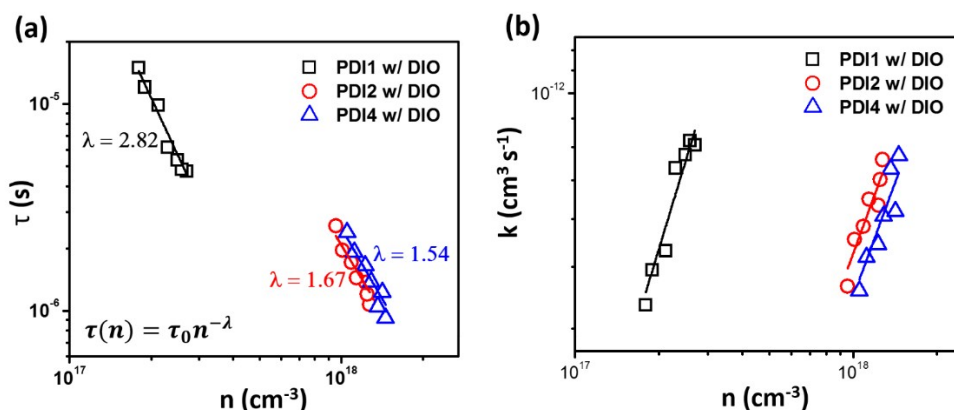


Figure S14. (a) Charge carrier lifetime (τ) derived versus charge carrier density (n) and (b) charge recombination coefficient (k) versus n for PTB7-Th:PDI1, PTB7-Th:PDI2 and PTB7-Th:PDI4 solar cells with DIO. Open scattered points represent experimental data points, while the solid line corresponds to the fit on the data as described in [11].

References

- [1] Y. Huang, J. Hu, W. Kuang, Z. Wei, C. F. Faul, *Chem. Commun.* 2011, **47**, 5554.
- [2] Q. Yan, D. Zhao, *Org. Lett.* 2009, **11**, 3426.
- [3] W. Jiang, L. Ye, X. Li, C. Xiao, F. Tan, W. Zhao, J. Hou, Z. Wang, *Chem. Commun.* 2014, **50**, 1024.
- [4] J. Lee, R. Singh, D. H. Sin, H. G. Kim, K. C. Song, K. Cho, *Adv. Mater.* 2016, **28**, 69-76.
- [5] Q. F. Yan, Y. Zhou, Y. Q. Zheng, J. Pei, D. H. Zhao, *Chem. Sci.* 2013, **4**, 4389.
- [6] H. Zhou, L. Yang, A. C. Stuart, S. C. Price, S. Liu, W. You, *Angew. Chem. Int. Ed.* 2011, **50**, 2995.
- [7] M. J. Frisch, *et al. Gaussian 09, Revision A.02*, Gaussian, Inc., Wallingford CT, 2009.
- [8] Y. X. Xu, C. C. Chueh, H. L. Yip, F. Z. Ding, Y. X. Li, C. Z. Li, X. Li, W. C. Chen, A. K. Y. Jen, *Adv. Mater.* 2012, **24**, 6356.
- [9] R. Singh, E. A.-Sarduy, Z. Kan, T. Ye, R.C.I. MacKenzie, P. E. Keivanidis, *J. Mater. Chem. A* 2014, **2**, 14348.
- [10] T. Ye, R. Singh, H. -J. Butt, G. Floudas, P. E. Keivanidis, *ACS Appl. Mater. Interfaces* 2013, **5**, 11844.
- [11] D. Spoltore, W. D. Oosterbaan, S. Khelifi, J. N. Clifford, A. Viterisi, E. Palomares, M. Burgelman, L. Lutsen, D. Vanderzande and J. Manca, *Adv. Energy Mater.*, 2013, **3**, 466-471.